THE JOURNAL OF PHYSICAL CHEMISTRY C

Article

pubs.acs.org/JPCC

Tuning Electronic Properties and Band Alignments of Phosphorene Combined With $MoSe_2$ and WSe_2

Daniel S. Koda,*,† Friedhelm Bechstedt,*,‡ Marcelo Marques,*,† and Lara K. Teles*,†

†Grupo de Materiais Semicondutores e Nanotecnologia, Instituto Tecnológico de Aeronáutica, DCTA, 12228-900 São José dos Campos, Brazil

‡Institut für Festkörpertheorie und -optik, Friedrich-Schiller-Universität, Max-Wien-Platz 1, D-07743 Jena, Germany

Supporting Information

ABSTRACT: Stacks of two-dimensional crystals in van der Waals heterostructures pave the way to novel applications in electronics and optoelectronics. Based on first-principles calculations, we study heterobilayers constructed with phosphorene on $MoSe_2$ and WSe_2. Both combinations are stable upon contact, while van der Waals interaction leads to a long-range structural bending, affecting electronic properties from phosphorene. Including quasiparticle effects, strong orbital overlaps are observed in the heterobilayers, influencing band offsets and, hence, emphasizing the importance of quasiparticle calculations over standard density functional theory ones. Interface effects also change the heterostructure type, modify local band gaps, and favor indirect transitions. To tailor the electronic properties of the heterostructures, interface interactions and external perturbations are taken into account through vertical pressures and electric fields. Uniaxial pressure strongly affects local direct gaps, and small electric fields can sweep band lineups and even change the heterostructure type. The studied features demonstrate the potential of bilayer systems for field-effect transistors, optoelectronic devices, and sensitive sensors.

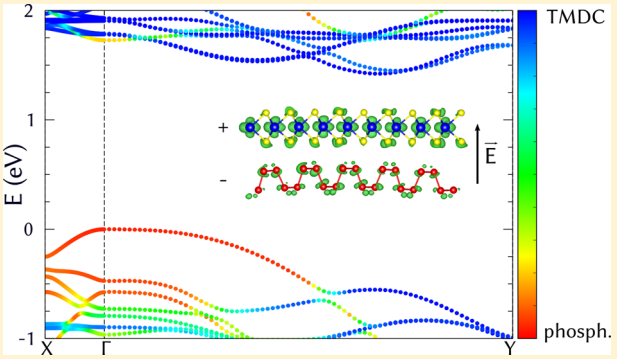

INTRODUCTION

Two-dimensional (2D) crystals such as graphene became the building blocks of layered structures for studying new physics and applications in novel devices.[1−3] The recent success in preparation of 2D monolayers and the discovery of their remarkable properties, including tunable band gaps[2] and sensitive structural properties,[3] greatly increased research interests in 2D systems. Nowadays, a trending 2D crystal is the monolayer black phosphorus, named phosphorene (Ph). This buckled single-layer crystal with a rectangular Bravais lattice is strongly anisotropic[4] and has an on−off ratio up to 10 000.[5] Furthermore, black phosphorus has a direct band gap depending on the number of layers and up to 1.51 eV in the monolayer case.[6] This new 2D crystal suggests application in solar cells, photosensors and atomically thin transistors. Transition metal dichalcogenides (TMDCs) are also popular within 2D physics. Molybdenum and tungsten dichalcogenides are examples for important 2D semiconductors, which present direct band gaps of 1.8 and 1.9 eV, respectively, in the visible frequency range,[2] tunable optical response[7] and low-power consumption for transistors.[8]

The variety of 2D crystals provides an ideal repository for their combination in heterojunctions. Systems made by stacking them vertically, known as van der Waals (vdW) heterostructures, are promising due to interesting electronic and optoelectronic features that go beyond the superposition of the properties from both layers.[9] Such heterojunctions have already been suggested or even prepared by 2D crystals weakly bonded with phosphorene including graphene/Ph bilayers,[10] Ph/MoS_2 diodes,[11] and phosphorene encapsulated with hexagonal boron-nitride.[12]

Most important for heterojunctions are the band offsets at the interface, especially for band-engineered devices. Comparisons between the natural band discontinuities (those based only on the original electron affinity rule[13]) of 2D crystals and the band lineups in heterosystems demonstrate that the weak interlayer bonding between the two layers and the formation of quantum dipoles[14,15] may influence the electronic properties of the constituents of the interface.[16−18] Thus, natural band offsets are not sufficient to accurately describe the heterojunction. Additionally, out-of-plane alignments, such as interlayer twist, vertical displacements and external pressure may be responsible for significant changes in vdW interactions between the two 2D crystals.[19−21] The modeling of a realistic heterointerface, which takes into account the influence of long-range stacking orders and vdW-induced structure variations, could lead to substantial modifications in electronic structures of the materials in the heterojunction.

Received: November 1, 2016
Revised: January 10, 2017
Published: January 23, 2017

DOI: 10.1021/acs.jpcc.6b10976
J. Phys. Chem. C 2017, 121, 3862−3869

In this work, we analyze structural and electronic properties of realistic Ph/$MoSe_2$ and Ph/WSe_2 combinations by *ab initio* calculations (see section Computational Details). Results show that both bilayer systems are stable upon contact and interact weakly via vdW bonds. Structural relaxations lead to a long-range warping of the phosphorene layer in the armchair direction in both bilayer systems due to local vdW bonds and the mechanical flexibility of phosphorene. Interlayer interactions also increase the phosphorene band gap by 0.2 eV, and a strong orbital overlap with the TMDC layer changes heterostructure types. A discussion on the nature of band offsets within interacting systems is raised and we propose a criterion to define band discontinuities in these cases. The relevance of density functional theory (DFT) with quasiparticle corrections is highlighted by comparing the results with semilocal DFT calculations. We further extend the investigations to tune the heterobilayer bands by means of a vertical electric field and piezoelectric effects. The band hybridization can be modulated by the application of a vertical electric field for which a direct to indirect gap transition is observed in phosphorene. Uniaxial vertical pressures also tune the local band gaps and band offsets in the heterosystem. We demonstrate that both studied heterobilayers are sensitive to external pressures and that small electric fields can be used for fine-control of band offsets, suggesting application in electronic sensors and tunable optoelectronic devices.

COMPUTATIONAL DETAILS

The calculations are performed within the DFT[22,23] by using the Projector Augmented Plane-Wave (PAW) method[24,25] as implemented in Vienna Ab-Initio Simulation Package (VASP).[26,27] The description of exchange and correlation (XC) was conducted using the Perdew–Burke–Ernzerhof (PBE) functional within the generalized gradient approximation (GGA).[28] van der Waals interaction was taken in account using the optB86b functional[29] to predict structural and energy parameters more accurately when compared with its counterparts.[29−31] The kinetic energy cutoff for the plane waves is restricted to 500 eV and integrations over the 2D Brillouin zone (BZ) are performed using a 3 × 12 × 1 Γ-centered Monkhorst–Pack k-points mesh[32] for supercells. The repeated slab method is applied to simulate individual 2D crystals[33] and the relative arrangement of the two 2D crystals in the heterostructures was obtained according to the method for finding coincidence lattices in ref 34. A vacuum of 15 Å thickness is employed to ensure no unphysical interaction in the stacking direction. All structural parameters are calculated first finding the energy minimum with a stopping criterion of 10^{-5} eV for the energy convergence and then relaxing the atomic positions until the Hellmann–Feynman forces on atoms were smaller than 1 meV/Å. Heterostructure investigations are performed after fixing the parameters of the most stable structural geometry of each monolayer and applying necessary strains to make the systems commensurate.

For the electronic properties we approximately take the quasiparticle corrections into account by applying a XC hybrid functional HSE06[35−38] to compute the electronic band states. This XC approach simulates the important spatial nonlocality of the quasiparticle self-energy in GW approximation.[39]

Visualizations of supercells and structures were done with the software VESTA.[40]

RESULTS AND DISCUSSION

The simulated structures of the bilayer Ph/$MoSe_2$ are depicted in Figure 1. The geometry of Ph/WSe_2 is similar and, therefore, not displayed. We start from the lattice parameters, optimized using vdW corrections via the optB86b functional,[29] a_{arm} = 4.504 Å in the armchair direction and a_{zig} = 3.305 Å in zigzag direction for the phosphorene, and a = 3.301 Å for the hexagonal $MoSe_2$ and a = 3.296 Å for WSe_2. The vdW heterostructure supercell is constructed from nonprimitive 5 × 1 (armchair × zigzag) unit cells of phosphorene and 4 × 1

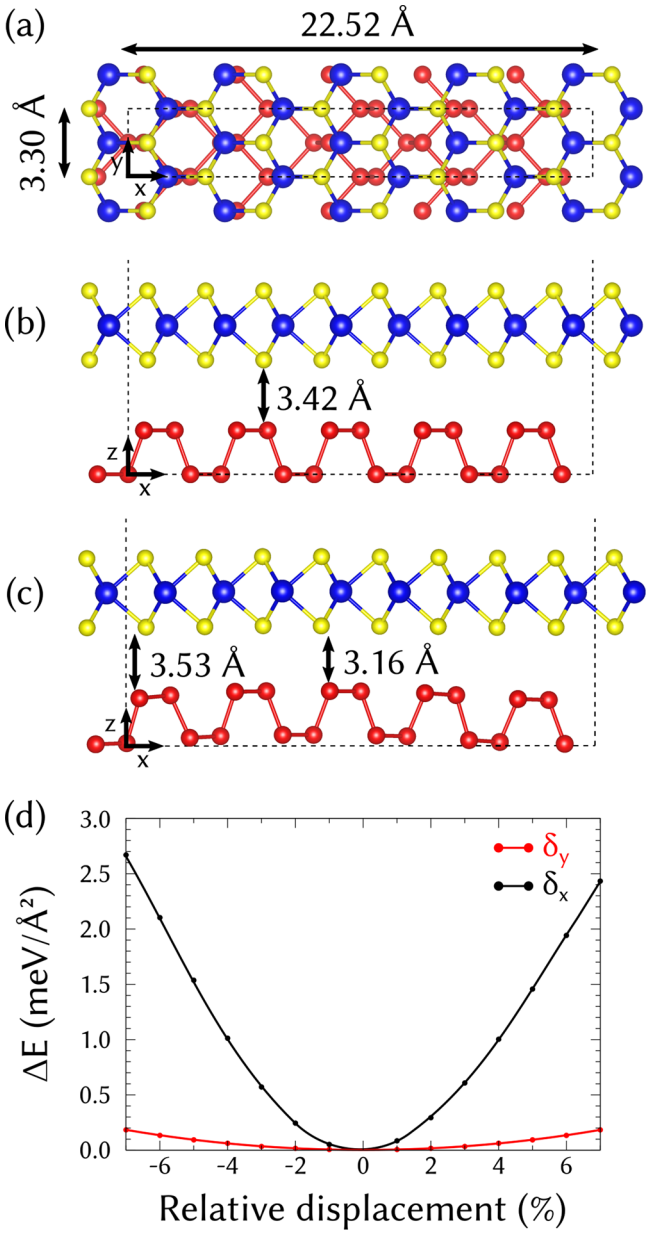

Figure 1. Supercell used for simulating the Ph/$MoSe_2$ heterointerface. A (a) top and (b) side view before structural relaxation depict the flat interface between the two materials. (c) After minimization of atomic forces, the phosphorene moves toward the $MoSe_2$ layer. Phosphorus, selenium, and molybdenum atoms are represented with gray, yellow, and blue atoms, respectively, and the supercell boundary is displayed by black dashed lines. (d) Decrease of energy (ΔE) of the bilayer system when small relative displacements are made in the armchair (δ_x) and zigzag (δ_y) directions.

DOI: 10.1021/acs.jpcc.6b10976
J. Phys. Chem. C 2017, 121, 3862−3869

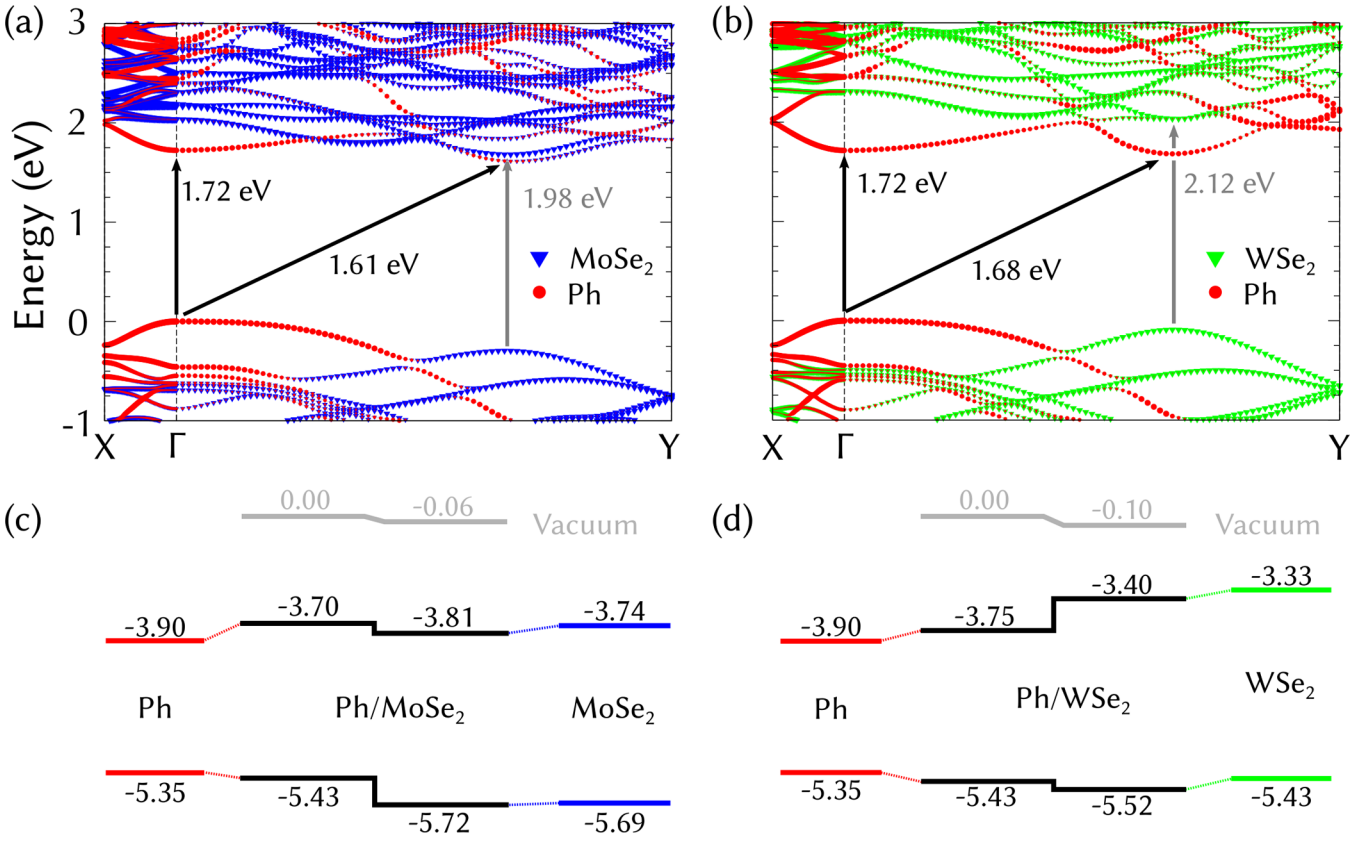

Figure 2. Band structures of (a) Ph/$MoSe_2$ and (b) Ph/WSe_2 heterostructures. Contributions from phosphorus atoms are shown with red circles and from the $MoSe_2$ (WSe_2) monolayer are displayed with blue (green) triangles. The size of the symbols specifies the relative contribution from each monolayer to the band formation. The top of the phosphorene valence band is used as energy zero. Band alignments of (c) Ph/$MoSe_2$ and (d) Ph/WSe_2 heterostructures with respect to the vacuum level. Results for freestanding and combined 2D crystals are displayed. All energies are shown in eV.

rectangular unit cells of $MoSe_2$ (WSe_2), resulting in an armchair lattice parameter of 22.519 Å for both supercells. Rotations of two cells against each other are less favorable, as shown by the coincidence lattice method.[34] To further investigate structural parameters from these heterobilayer systems, we first apply the necessary strain to make the phosphorene system commensurate on the $MoSe_2$ (WSe_2) layer.[34] This means that small nonbiaxial strains of −1.54% (−1.39%) in the armchair direction and 0.13% (0.28%) in the zigzag direction are applied to the materials, leaving the phosphorene intact. This strain slightly changes the $MoSe_2$ (WSe_2) electronic properties by increasing the band gap from 1.95 eV (2.11 eV) to 2.04 eV (2.17 eV) and by allowing a transition from a direct to an indirect band gap, as expected for a small compressive strain.[41] However, the difference between direct and indirect band gaps of the TMDC layers is smaller than 0.01 eV (0.02 eV). Hence, changes observed in electronic properties of the strained materials still allow us to investigate the electronic properties of the heterobilayers without incurring large deviations from the freestanding case, even when only one of the heterostructure constituents is strained to form the commensurate system (see Figure S1).

Structural parameters are computed starting with a given interlayer distance in both bilayer systems by means of total energy calculations. First, the atoms are kept fixed in their positions within the layer, and the distance between the layers is varied. This leads to a favorable interlayer distance of 3.415 Å (3.506 Å) for the Ph/$MoSe_2$ (Ph/WSe_2) system, in agreement with typical lengths between vdW bonded atoms and layers.[42,43] Then, the atoms and the volume of the supercell are allowed to relax until the Hellmann−Feynman forces are smaller than 1 meV/Å. This leads to a more stable equilibrium configuration, which moves the phosphorene toward the $MoSe_2$ (WSe_2) layer, creating a spatial distribution for the interlayer distance in the armchair direction, resulting in a bending, as shown in Figure 1c. These out-of-plane displacements are responsible for a stabilizing effect provided by the weak vdW interaction in the heterojunction and have been recently theoretically explained.[44] Atomic displacements occur in the armchair direction, which has been predicted as being the preferential direction for dislocations due its out-of-plane flexibility.[45] The resulting armchair warping is only observed due to the long-range periodicity of the supercell in this direction, which is 4 times longer than the TMDC unit cell. Doubling the supercell length in the armchair direction does not change the warping. Weak interlayer interactions, therefore, compensate for the strain induced on the structure. By comparing panels a and c of Figure 1, it can be seen that the region in which the interlayer distance between phosphorene and the TMDC layer is equivalent to an AB stacking order, while this distance is maximum in the region with an equivalent AA stacking. These local interlayer distances are compatible with AA and AB-stacked phosphorene layers.[46]

The stability of the heterobilayer systems is further enhanced by expanding the lateral unit cell, verified by the lowering of their total energy. Joint cells created by relaxing both structures

DOI: 10.1021/acs.jpcc.6b10976
J. Phys. Chem. C 2017, 121, 3862−3869

have an armchair lattice parameter of 22.734 Å (22.740 Å) and a zigzag lattice parameter of 3.299 Å (3.297 Å) for the Ph/$MoSe_2$ (Ph/WSe_2) heterojunction. The Moiré pattern length calculated for these systems is 21.2 Å, in agreement with the supercell length for the commensurate system. This corresponds to phosphorene strained by about 1.0% in the armchair direction and −0.2% in the zigzag direction in both cases. The armchair strain for $MoSe_2$ (WSe_2) is reduced to −0.6% (−0.4%), and the zigzag strain is negligible in the heterojunction situation. In addition, the phosphorene is bended in the armchair direction by about 10%. The increased stability by straining phosphorene can be easily understood when one compares the calculated stress tensor from phosphorene with that of $MoSe_2$ or WSe_2. The natural flexibility of monolayer phosphorene in the armchair direction (in-plane stiffness of 26 N/m)[47,48] with respect to in-plane strain is superior to that from the studied TMDCs (101 N/m for $MoSe_2$ and 112 N/m for WSe_2).[41] It lowers the energy of the combined system and reduces atomic forces.

By varying the interlayer distance, it is possible to infer, from the total energy calculations, the binding energy of the two systems represented as a gain of total energy per unit area, more precisely the difference between the energy of the heterobilayer and the energy of the isolated monolayers. For the flat phosphorene over $MoSe_2$ (WSe_2), the binding energy is 23.4 meV/Å^2 (23.8 meV/Å^2), which is a reasonable value for bilayer systems involving TMDCs.[34,49] The structural relaxation, which includes small volume changes, and the bending of the phosphorene, increases the binding energy, as this favors vdW interactions on the interface. In this case, the binding energy slightly increases to 24.9 meV/Å^2 (25.2 meV/Å^2). For the matter of comparison, we calculated the binding energy for the AB-stacked bilayer phosphorene as being 31.9 meV/Å^2. This demonstrates the stability of the vdW-bonded bilayer system, as with stacking displayed in Figure 1a and its enhanced binding via out-of-plane displacements. From the lowest energy configuration, we further moved laterally one layer with respect to the other considering small relative displacements in the armchair (δ_x) and zigzag (δ_y) directions to make sure we really found the minimum energy configuration. This local stability is shown in Figure 1d.

Electronic properties of the isolated and bilayer systems were investigated using the exchange-correlation hybrid functional HSE06.[35−38] Its spatial nonlocality simulates an important property of the quasiparticle self-energy. It increases the gaps and interband distances in comparison to local or semilocal DFT results. Band structures of the bilayer systems are shown in Figure 2a,b. Small differences between band structures of the flat freestanding and warped phosphorene over $MoSe_2$ (WSe_2) are due to strain effects on phosphorene created by volume relaxation (Figure S2). The local direct band gap of phosphorene increases from 1.54 eV in the strained and isolated monolayer to 1.72 eV (1.72 eV) when put in contact with $MoSe_2$ (WSe_2) due to vdW interactions and orbital overlapping in the interface. The increase in the band gap at Γ can be explained by the high sensitivity of the phosphorene conduction band minimum (CBM), created primarily by p_z orbitals, upon contact with other atomic layers. In our case, the overlap of $MoSe_2$ (WSe_2) d_{z^2} and p_z orbitals with those from the phosphorene layer defines about 13% (12%) of the orbital character of the joint conduction band. On the other hand, the top of the valence band overlaps little with the TMDC layer, with 4% (3%) of contribution from $MoSe_2$ (WSe_2), shifting down the VBM level and further opening the gap. This shift occurs only in regions in the k-space where the conduction band of phosphorene is generated by p_z orbitals, and this relative overlap agrees quantitatively with the band gap increase experienced by the phosphorene layer as also observed for other heterostructures containing phosphorene.[10,21,50,51]

The second minimum in the phosphorene conduction band is originally only 0.26 eV above the global conduction band minimum. However, the uniaxial strain in the armchair direction reduces this difference, as also predicted theoretically from other work.[52] Since it is produced by p_x and p_y orbitals (see Figure S3), it does not suffer an energy increase when put in contact with the TMDC layer. However, this second minimum experiences a strong orbital overlap with the $MoSe_2$ layer due to charge transfer and band superposition, as shown by the relative contributions from different layers to the conduction band in Figure 2a. At about 0.70 Γ-Y, the CBM has a composition of 36% Ph and 64% $MoSe_2$, thus showing that the probability density to find an electron with an energy equal to the heterobilayer CBM is greater within $MoSe_2$. This balance of overlapping is only observed when quasiparticle effects are taken into account, since local or semilocal DFT calculations show that the second minimum in the conduction band is made by 64% phosphorene and 36% $MoSe_2$.

This discussion raises a quantum-mechanical criterion to define a band edge of vdW interfaces within hybrid systems. We define band edges as local energy minima (maxima) near the gap in the k-space, which belong to the crystal where the probability density to find the electron (hole) with this specific energy is maximum. If such a definition, including the orbital character of the band edges, is possible, one can still introduce "real" band discontinuities in the electronic band structure of heterosystems, even if they are not well energetically separated. Band discontinuities can also be represented by states localized at the two sides of the interface. This interpretation, derived from the electron (hole) wave function, allows the analysis of hybrid structures by localizing the electron (hole), instead of simply relying on the natural band discontinuities. It is also coherent with cases in which little orbital overlap is seen and helps to define a standard to vdW heterostructures with overlapping electronic properties.

The energy separations of the band edges at both sides of the heterointerface can be interpreted as "natural" band discontinuities or offsets. By setting the vacuum level as reference for the electrostatic potential, natural band discontinuities are calculated and compared with the real ones for both studied systems. These results are summarized in Figure 2c,d. Band offsets for both heterobilayers, calculated with the criterion discussed above, deviate from their natural band discontinuities up to 0.2 eV. Hybridization leads to a considerable change in band lineups (black lines in Figure 2c,d) for Ph/$MoSe_2$, in which the heterostructure experiences a type I to type II transition. Ph/WSe_2 systems preserve the type I of the heterostructure expected from the natural band discontinuities, since band superpositions do not affect directly the phosphorene CBM. Shifts in band levels are further enhanced by charge transfer between the two layers. By comparing the vacuum level from both sides of the interface, a potential barrier is observed due to the formation of a dipole on the interface. In both systems, the TMDC layer is depleted from electrons, which shifts downward its bands with respect to the vacuum level, while phosphorene receives electrons and becomes negatively charged. For Ph/$MoSe_2$ (Ph/WSe_2), the calculated

DOI: 10.1021/acs.jpcc.6b10976
J. Phys. Chem. C 2017, 121, 3862−3869

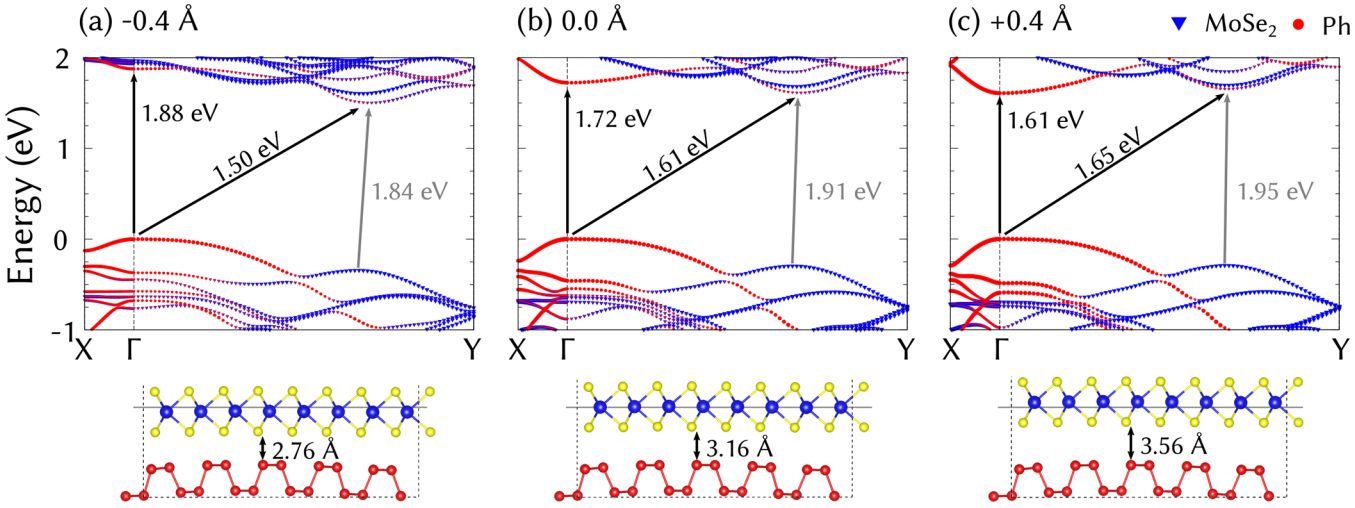

Figure 3. Band structures for the Ph/$MoSe_2$ heterobilayer when the vdW gap length is (a) reduced by 0.4 Å, (b) kept constant, and (c) increased by 0.4 Å with respect to the equilibrium position. Red and blue markers depict orbital contributions from the phosphorene and $MoSe_2$ layers, respectively. The top of the valence band is taken as reference.

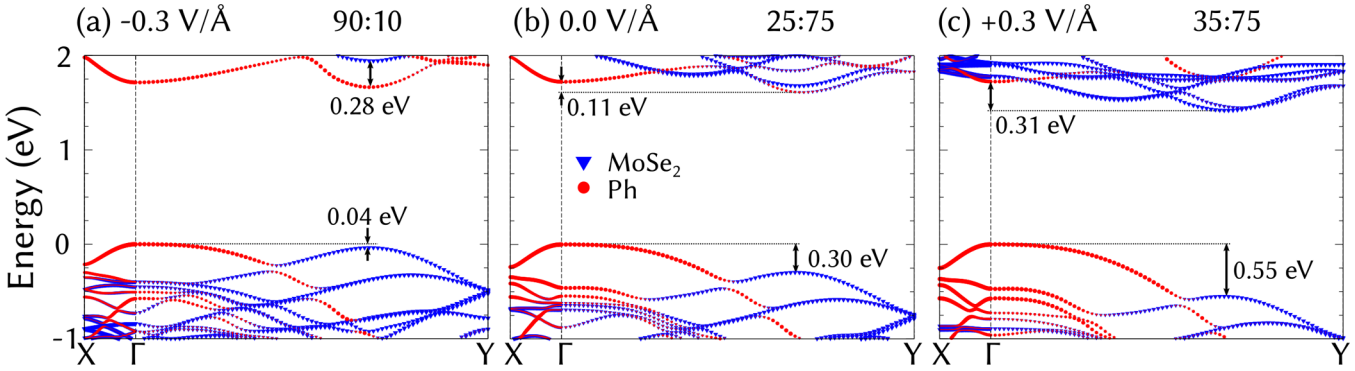

Figure 4. Band structures for the Ph/$MoSe_2$ heterobilayer when an electric field of (a) −0.3 V/Å, (b) 0.0 V/Å, and (c) + 0.3 V/Å is applied in the z direction. The ratios $\Delta E_c/(\Delta E_g)$ and $\Delta E_v/(\Delta E_g)$ are also given. Red and blue markers depict bands formed by orbitals from the phosphorene and $MoSe_2$ layers, respectively. The top of the valence band of each combined system is taken as reference.

band offsets are given by ΔE_v = 0.30 eV (0.09 eV), the valence band offset (VBO), and ΔE_c = 0.11 eV (0.35 eV), the conduction band offset (CBO).

Influences of quasiparticle (QP) corrections on the direct or indirect band gaps of phosphorene within the heterostructures have also been investigated. A comparison between free-standing band discontinuities and heterostructure band offsets from HSE06 and DFT calculations are shown in Tables S1 and S2. Besides the gap results, which indicate large QP openings for WSe_2 and Ph, also the natural band discontinuities in HSE06 ΔE_v = 0.30 eV (0.09 eV) and ΔE_c = 0.11 eV (0.35 eV) vary compared to ΔE_v^{DFT} = 0.31 eV (0.16 eV), and ΔE_c^{DFT} = 0.21 eV (0.44 eV) for the Ph/$MoSe_2$ (Ph/WSe_2) heterostructure.

One way to tune the sensitive electronic properties from phosphorene is through the piezoelectric effect and charge redistribution in the heterointerface, which have been reported both theoretically[21] and experimentally[53,54] for 2D crystals and other vdW heterostructures. By changing the vdW distances in stacks, it is possible to vary the band gaps from the constituents of the heterostructure due to the modification of the interlayer interaction. We displaced the $MoSe_2$ (WSe_2) layer up to ±0.4 Å from the equilibrium distance in the warped phosphorene configuration. The corresponding uniaxial pressure along the interface normal direction drastically affects the direct band gap of phosphorene, as summarized in Figure 3 (Figure S4) for the Ph/$MoSe_2$ (Ph/WSe_2) system. The direct band gaps increase when the layers in the heterostructure are put closer, due to more intense interlayer interaction and orbital overlapping (see Figures S5, S9, and S10). The same physical reason is responsible for shrinking the direct band gap in phosphorene when the two layers have a larger distance than the equilibrium one. Increasing the separation between the two layers leads, asymptotically, to the isolated monolayer case. This is also observed in the Ph/WSe_2 heterobilayer system (Figures S4 and S10). On the other hand, the band gaps of the $MoSe_2$ and WSe_2 layers decrease when the heterobilayer is compressed and increase with the layer separation. This modulation can significantly affect the direct gap of the heterobilayer, which is an interesting feature for optoelectronic sensors and devices, as well as tune band offsets and transport properties by employing mechanical pressure.

Another possibility to tune band alignments at the Ph/$MoSe_2$ or Ph/WSe_2 interfaces is to apply a vertical external electric field parallel to the stacking direction. This leads not only to a band alignment, but also a heterostructure character depending on the magnitude of the electric field. For both cases, we analyzed small electric fields ranging from −0.4 V/Å to 0.4 V/Å

DOI: 10.1021/acs.jpcc.6b10976
J. Phys. Chem. C 2017, 121, 3862−3869

with steps of 0.1 V/Å. Figure 4 (Figure S6) illustrates how electronic properties of Ph/$MoSe_2$ (Ph/WSe_2) are influenced by an electric field. When a field is applied in the $-z$ direction, the CBO of the heterostructure increases while reducing the VBO. The charge redistribution imposed by the external electric perturbation leads to a band shift, which can also be interpreted as a bias in the Fermi level on each side of the interface. In the case of the field in the $-z$ direction, this occurs due to the depletion of electrons from Ph by the external electric field, shifting its bands downward. The opposite behavior of the band offsets happens for $MoSe_2$ and WSe_2. The $MoSe_2$-derived conduction band at about 0.70 Γ−Y moves down in energy, while the Ph one shifts toward the vacuum level. As a consequence, a joint band with partial Ph and $MoSe_2$ character appears (see Figure S11). For higher field strengths, the Ph/$MoSe_2$ heterostructure returns to a type I character due to this controlled interaction. The crossing point with the vanishing CBO is near −0.1 V/Å, in which the electron wave function displays about 50% probability to find an electron when projected onto each layer. In Figure S7, the transition of the Ph/WSe_2 heterostructure character close to −0.1 V/Å is illustrated in a more pronounced manner due to the smaller VBO, while the transition induced by orbital overlap happens for fields close to 0.25 V/Å. If, on the other hand, an electric field is applied to the system in the $+z$-direction, the TMDC layer is depleted from electrons and a negative charge accumulates in the Ph layer. This increases both the VBO and CBO for the type II heterostructure and enhances interactions between the two systems. The local energy gaps depend on the application of an electric field due to the tunable band hybridization (Figure S12). Band offsets defined by local direct gaps, useful for optoelectronics, are also modulated by an electric field, as shown in Figure S8. For the Ph/$MoSe_2$ (Ph/WSe_2) system, two transitions between heterostructure types are observed for electric fields close to −0.35 V/Å and −0.5 V/Å (−0.1 V/Å and 0.35 V/Å) when considering band offsets defined by direct gaps. Figures S7 and S8 also demonstrate the relevance of quasiparticle corrections when calculating band offsets, since DFT calculations do not correctly describe the band hybridization and transitions between heterostructure types under the application of electric fields when examined closely with HSE06 calculations. The former also underestimates the slope of the band offsets with respect to the applied vertical field when compared to the latter. The possibility to control band alignments in heterostructures by vertical fields and enhancement of orbital overlap is fascinating. It paves the way to control carrier injection from one subsystem to another. This broadens possibilities for the construction of field-effect transistors with channels made from atom-thick layers. Moreover, the controlled type II character with electron−hole separation across the heretointerface makes both Ph/$MoSe_2$ and Ph/WSe_2 bilayers suitable for photovoltaic applications.

CONCLUSION

In summary, we have analyzed two heterobilayers of Ph/$MoSe_2$ and Ph/WSe_2 by first-principles calculations. We demonstrate that the systems are stable upon contact and that an interlayer structural bending of 10% is observed in Ph due to vdW interactions. By calculating electronic structures within the approximate quasiparticle picture HSE06, we found an increase of 0.18 eV in the phosphorene band gap and a pronounced orbital overlap, which changes the heterostructure type within Ph/$MoSe_2$ and favors an indirect gap transition in Ph/WSe_2. A definition of band offsets for hybridized systems is proposed, according to which band discontinuities are analyzed together within charge transfer and hybridization mechanisms. Significant differences between band offsets calculated with DFT and HSE06 demonstrate the importance of quasiparticle corrections within vdW heterostructures. Electronic properties of the heterobilayers are tuned via application of external pressure and electric field. We demonstrate the sensitivity of the heterostructures to an external pressure, which modulates band alignments and local direct gaps by up to 0.15 eV for uniaxial vertical strains smaller than 13%. Moreover, electric fields smaller than 0.4 V/Å can tune the band alignments and control the hybridization between the systems. Whereas strain modulates the band gaps and band offsets in a monotonic way, electric fields along the combined systems can also change the heterostructure character from type I to type II. The studied heterobilayer systems may be useful for applications in optoelectronics and in FET devices.

ASSOCIATED CONTENT

Supporting Information

The Supporting Information is available free of charge on the ACS Publications website at DOI: 10.1021/acs.jpcc.6b10976.

Figure S1: A comparison between strained and unstrained band structures for $MoSe_2$ and WSe_2; Figure S2: A comparison between band structures when phosphorene is warped or kept flat; Figure S3: Band structures for the freestanding phosphorene and $MoSe_2$ projected onto atomic orbitals; Figure S4: Comparison between band structures for the Ph/WSe_2 system under different vertical pressures; Figure S5: Direct gap of phosphorene as a function of the interlayer distance change with respect to the equilibrium one; Figure S6: Comparison between band structures for the Ph/WSe_2 system under different electric fields; Figure S7: Dependence of band offsets with vertical electric fields, showing the voltage for which there is a transition for the heterostructures from type I to type II; Figure S8: Dependence of band offsets, defined by local direct gaps, with vertical electric fields, showing the voltage for which there is a transition for the heterostructures from type I to type II; Figure S9: Band structure composition/character as projected onto Ph and $MoSe_2$ monolayers, under different vertical pressures; Figure S10: Band structure composition/character as projected onto Ph and WSe_2 monolayers, under different vertical pressures; Figure S11: Band structure composition/character as projected onto Ph and $MoSe_2$ monolayers, under different electric fields; Figure S12: Band structure composition/character as projected onto Ph and WSe_2 monolayers, under different electric fields; Figure S13: Differential and integrated charge densities of the Ph/$MoSe_2$ and Ph/WSe_2 heterobilayer systems; Table S1: Values for the conduction band minimum, valence band maximum, direct and indirect energy gaps; Table S2: Values for the conduction band offset and valence band offset, with their percentage with respect to ΔE_g (PDF)

AUTHOR INFORMATION

Corresponding Authors

*E-mail: danielskoda@aluno.ita.br.

DOI: 10.1021/acs.jpcc.6b10976
J. Phys. Chem. C 2017, 121, 3862−3869

*E-mail: friedhelm.bechstedt@uni-jena.de.
*E-mail: mmarques@ita.br.
*E-mail: lkteles@ita.br.

ORCID

Lara K. Teles: 0000-0002-8713-2094

Notes

The authors declare no competing financial interest.

■ ACKNOWLEDGMENTS

The authors acknowledge the National Laboratory for Scientific Computing (LNCC/MCTI, Brazil) for providing HPC resources of the SDumont supercomputer, which have contributed to the research results reported within this paper. This work was funded by the Brazilian agencies Conselho Nacional de Desenvolvimento Científico e Tecnológico (grant no. 311060/2013-7) and Coordenação de Aperfeiçoamento de Pessoal de Nível Superior (Programa Professor Visitante do Exterior, grant no. 88881.068355/2014-01 and scholarship grant) within the program Science Without Borders.

■ REFERENCES

(1) Butler, S. Z.; Hollen, S. M.; Cao, L.; Cui, Y.; Gupta, J. A.; Gutiérrez, H. R.; Heinz, T. F.; Hong, S. S.; Huang, J.; Ismach, A. F.; et al. Progress, Challenges, and Opportunities in Two-Dimensional Materials Beyond Graphene. *ACS Nano* **2013**, *7*, 2898−2926.
(2) Wang, Q. H.; Kalantar-Zadeh, K.; Kis, A.; Coleman, J. N.; Strano, M. S. Electronics and optoelectronics of two-dimensional transition metal dichalcogenides. *Nat. Nanotechnol.* **2012**, *7*, 699−712.
(3) Xu, M.; Liang, T.; Shi, M.; Chen, H. Graphene-like two-dimensional materials. *Chem. Rev.* **2013**, *113*, 3766−3798.
(4) Fei, R.; Yang, L. Strain-engineering the anisotropic electrical conductance of few-layer black phosphorus. *Nano Lett.* **2014**, *14*, 2884−2889.
(5) Liu, H.; Neal, A. T.; Zhu, Z.; Luo, Z.; Xu, X.; Tománek, D.; Ye, P. D. Phosphorene: an unexplored 2D semiconductor with a high hole mobility. *ACS Nano* **2014**, *8*, 4033−4041.
(6) Qiao, J.; Kong, X.; Hu, Z.-X.; Yang, F.; Ji, W. High-mobility transport anisotropy and linear dichroism in few-layer black phosphorus. *Nat. Commun.* **2014**, *5*, 4475.
(7) Tongay, S.; Zhou, J.; Ataca, C.; Lo, K.; Matthews, T. S.; Li, J.; Grossman, J. C.; Wu, J. Thermally driven crossover from indirect toward direct bandgap in 2D semiconductors: MoSe2 versus MoS2. *Nano Lett.* **2012**, *12*, 5576−5580.
(8) Radisavljevic, B.; Radenovic, A.; Brivio, J.; Giacometti, V.; Kis, A. Single-layer MoS2 transistors. *Nat. Nanotechnol.* **2011**, *6*, 147−150.
(9) Geim, A.; Grigorieva, I. Van der Waals heterostructures. *Nature* **2013**, *499*, 419−425.
(10) Padilha, J.; Fazzio, A.; da Silva, A. J. Van der Waals heterostructure of phosphorene and graphene: Tuning the Schottky barrier and doping by electrostatic gating. *Phys. Rev. Lett.* **2015**, *114*, 066803.
(11) Deng, Y.; Luo, Z.; Conrad, N. J.; Liu, H.; Gong, Y.; Najmaei, S.; Ajayan, P. M.; Lou, J.; Xu, X.; Ye, P. D. Black phosphorus-monolayer MoS2 van der Waals heterojunction p-n diode. *ACS Nano* **2014**, *8*, 8292−8299.
(12) Chen, X.; Wu, Y.; Wu, Z.; Han, Y.; Xu, S.; Wang, L.; Ye, W.; Han, T.; He, Y.; Cai, Y. High-quality sandwiched black phosphorus heterostructure and its quantum oscillations. *Nat. Commun.* **2015**, *6*, 7315.
(13) Anderson, R. Experiments on Ge-GaAs heterojunctions. *Solid-State Electron.* **1962**, *5*, 341−351.
(14) Tersoff, J. Theory of semiconductor heterojunctions: The role of quantum dipoles. *Phys. Rev. B: Condens. Matter Mater. Phys.* **1984**, *30*, 4874−4877.
(15) Schlaf, R.; Lang, O.; Pettenkofer, C.; Jaegermann, W.; Armstrong, N. R. Experimental determination of quantum dipoles at semiconductor heterojunctions prepared by van der Waals epitaxy: Linear correction term for the electron affinity rule. *J. Vac. Sci. Technol., A* **1997**, *15*, 1365−1370.
(16) Kang, J.; Tongay, S.; Zhou, J.; Li, J.; Wu, J. Band offsets and heterostructures of two-dimensional semiconductors. *Appl. Phys. Lett.* **2013**, *102*, 012111.
(17) Wei, W.; Dai, Y.; Huang, B. Hybridization Effects between Silicene/Silicene Oxides and Ag (111). *J. Phys. Chem. C* **2016**, *120*, 20192−20198.
(18) Zhou, S.; Zhao, J. Electronic Structures of Germanene on MoS2: Effect of Substrate and Molecular Adsorption. *J. Phys. Chem. C* **2016**, *120*, 21691−21698.
(19) Wang, Z.; Chen, Q.; Wang, J. Electronic Structure of Twisted Bilayers of Graphene/MoS2 and MoS2/MoS2. *J. Phys. Chem. C* **2015**, *119*, 4752−4758.
(20) van der Zande, A. M.; Kunstmann, J.; Chernikov, A.; Chenet, D. A.; You, Y.; Zhang, X.; Huang, P. Y.; Berkelbach, T. C.; Wang, L.; Zhang, F.; et al. Tailoring the Electronic Structure in Bilayer Molybdenum Disulfide via Interlayer Twist. *Nano Lett.* **2014**, *14*, 3869−3875.
(21) Huang, L.; Li, Y.; Wei, Z.; Li, J. Strain induced piezoelectric effect in black phosphorus and MoS2 van der Waals heterostructure. *Sci. Rep.* **2015**, *5*, 16448.
(22) Hohenberg, P.; Kohn, W. Inhomogeneous Electron Gas. *Phys. Rev.* **1964**, *136*, B864−B871.
(23) Kohn, W.; Sham, L. J. Self-Consistent Equations Including Exchange and Correlation Effects. *Phys. Rev.* **1965**, *140*, A1133−A1138.
(24) Blöchl, P. E. Projector augmented-wave method. *Phys. Rev. B: Condens. Matter Mater. Phys.* **1994**, *50*, 17953−17979.
(25) Kresse, G.; Joubert, D. From ultrasoft pseudopotentials to the projector augmented-wave method. *Phys. Rev. B: Condens. Matter Mater. Phys.* **1999**, *59*, 1758−1775.
(26) Kresse, G.; Furthmüller, J. Efficiency of ab-initio total energy calculations for metals and semiconductors using a plane-wave basis set. *Comput. Mater. Sci.* **1996**, *6*, 15−50.
(27) Kresse, G.; Furthmüller, J. Efficient iterative schemes for ab initio total-energy calculations using a plane-wave basis set. *Phys. Rev. B: Condens. Matter Mater. Phys.* **1996**, *54*, 11169−11186.
(28) Perdew, J. P.; Burke, K.; Ernzerhof, M. Generalized gradient approximation made simple. *Phys. Rev. Lett.* **1996**, *77*, 3865−3868.
(29) Klimeš, J.; Bowler, D. R.; Michaelides, A. Van der Waals density functionals applied to solids. *Phys. Rev. B: Condens. Matter Mater. Phys.* **2011**, *83*, 195131.
(30) Björkman, T. Testing several recent van der Waals density functionals for layered structures. *J. Chem. Phys.* **2014**, *141*, 074708.
(31) Zhu, J.; Schwingenschlögl, U. Silicene on MoS2: role of the van der Waals interaction. *2D Mater.* **2015**, *2*, 045004.
(32) Monkhorst, H. J.; Pack, J. D. Special points for Brillouin-zone integrations. *Phys. Rev. B* **1976**, *13*, 5188−5192.
(33) Bechstedt, F. *Principles of Surface Physics*; Springer-Verlag: Berlin, Heidelberg, 2003.
(34) Koda, D. S.; Bechstedt, F.; Marques, M.; Teles, L. K. Coincidence Lattices of 2D Crystals: Heterostructure Predictions and Applications. *J. Phys. Chem. C* **2016**, *120*, 10895−10908.
(35) Paier, J.; Marsman, M.; Hummer, K.; Kresse, G.; Gerber, I. C.; Ángyán, J. G. Screened hybrid density functionals applied to solids. *J. Chem. Phys.* **2006**, *124*, 154709.
(36) Paier, J.; Marsman, M.; Hummer, K.; Kresse, G.; Gerber, I.; Ángyán, J. Erratum:"Screened hybrid density functionals applied to solids"[J. Chem. Phys. 124, 154709 (2006)]. *J. Chem. Phys.* **2006**, *125*, 249901.
(37) Heyd, J.; Scuseria, G. E.; Ernzerhof, M. Hybrid functionals based on a screened Coulomb potential. *J. Chem. Phys.* **2003**, *118*, 8207−8215.
(38) Heyd, J.; Scuseria, G. E.; Ernzerhof, M. Erratum: "Hybrid functionals based on a screened Coulomb potential"[J. Chem. Phys. 118, 8207 (2003)]. *J. Chem. Phys.* **2006**, *124*, 219906.

DOI: 10.1021/acs.jpcc.6b10976
J. Phys. Chem. C 2017, 121, 3862−3869

(39) Bechstedt, F. *Many-Body Approach to Electronic Excitations*; Springer-Verlag: Berlin, Heidelberg, 2015.
(40) Momma, K.; Izumi, F. *VESTA*: a three-dimensional visualization system for electronic and structural analysis. *J. Appl. Crystallogr.* **2008**, *41*, 653−658.
(41) Guzman, D. M.; Strachan, A. Role of strain on electronic and mechanical response of semiconducting transition-metal dichalcogenide monolayers: An ab-initio study. *J. Appl. Phys.* **2014**, *115*, 243701.
(42) Kokott, S.; Pflugradt, P.; Matthes, L.; Bechstedt, F. Nonmetallic substrates for growth of silicene: an ab initio prediction. *J. Phys.: Condens. Matter* **2014**, *26*, 185002.
(43) Kokott, S.; Matthes, L.; Bechstedt, F. Silicene on hydrogen-passivated Si(111) and Ge(111) substrates. *Phys. Status Solidi RRL* **2013**, *7*, 538−541.
(44) Kumar, H.; Er, D.; Dong, L.; Li, J.; Shenoy, V. B. Elastic Deformations in 2D van der Waals Heterostructures and their Impact on Optoelectronic Properties: Predictions from a Multiscale Computational Approach. *Sci. Rep.* **2015**, *5*, 10872.
(45) Wang, G.; Loh, G. C.; Pandey, R.; Karna, S. P. Out-of-plane structural flexibility of phosphorene. *Nanotechnology* **2016**, *27*, 055701.
(46) Çakır, D.; Sevik, C.; Peeters, F. M. Significant effect of stacking on the electronic and optical properties of few-layer black phosphorus. *Phys. Rev. B: Condens. Matter Mater. Phys.* **2015**, *92*, 165406.
(47) Elahi, M.; Khaliji, K.; Tabatabaei, S. M.; Pourfath, M.; Asgari, R. Modulation of electronic and mechanical properties of phosphorene through strain. *Phys. Rev. B: Condens. Matter Mater. Phys.* **2015**, *91*, 115412.
(48) Wei, Q.; Peng, X. Superior mechanical flexibility of phosphorene and few-layer black phosphorus. *Appl. Phys. Lett.* **2014**, *104*, 251915.
(49) Björkman, T.; Gulans, A.; Krasheninnikov, A. V.; Nieminen, R. M. van der Waals bonding in layered compounds from advanced density-functional first-principles calculations. *Phys. Rev. Lett.* **2012**, *108*, 235502.
(50) Hu, T.; Hong, J. Anisotropic Effective Mass, Optical Property, and Enhanced Band Gap in BN/Phosphorene/BN Heterostructures. *ACS Appl. Mater. Interfaces* **2015**, *7*, 23489−23495.
(51) You, B.; Wang, X.; Zheng, Z.; Mi, W. Black phosphorene/monolayer transition-metal dichalcogenides as two dimensional van der Waals heterostructures: a first-principles study. *Phys. Chem. Chem. Phys.* **2016**, *18*, 7381−7388.
(52) Peng, X.; Wei, Q.; Copple, A. Strain-engineered direct-indirect band gap transition and its mechanism in two-dimensional phosphorene. *Phys. Rev. B: Condens. Matter Mater. Phys.* **2014**, *90*, 085402.
(53) da Cunha Rodrigues, G.; Zelenovskiy, P.; Romanyuk, K.; Luchkin, S.; Kopelevich, Y.; Kholkin, A. Strong piezoelectricity in single-layer graphene deposited on SiO2 grating substrates. *Nat. Commun.* **2015**, *6*, 7572.
(54) Zhu, H.; Wang, Y.; Xiao, J.; Liu, M.; Xiong, S.; Wong, Z. J.; Ye, Z.; Ye, Y.; Yin, X.; Zhang, X. Observation of piezoelectricity in free-standing monolayer MoS2. *Nat. Nanotechnol.* **2014**, *10*, 151−155.

DOI: 10.1021/acs.jpcc.6b10976
J. Phys. Chem. C 2017, 121, 3862−3869